Available online at www.sciencedirect.com
SCIENCE DIRECT®
International Journal of Pharmaceutics 275 (2004) 249–258
international journal of pharmaceutics
www.elsevier.com/locate/ijpharm

Effect of energy on propylene glycol aerosols using the capillary aerosol generator

X. Shen, M. Hindle*, P.R. Byron

Aerosol Research Group, Department of Pharmaceutics, Virginia Commonwealth University, Box 980533, 410 North 12th St., Richmond, VA 23298-0533, USA

Received 13 March 2003; received in revised form 11 September 2003; accepted 9 February 2004

Abstract

The CAG is being developed for pulmonary drug delivery. Liquids are pumped, heated and vaporized by the CAG, whence they nucleate and condense to form aerosols. This study characterized the effect of energy on the aerosolization process. With increasing energy, the CAG produced an increasing fine particle fraction (FPF) until "optimal aerosolization" was achieved between 40 and 45 J; this energy range agreed with that theoretically required to vaporize the dose of PG. Further increases in energy above this optimal range did not improve PG's aerosolization efficiency. Based on the energy, FPF and temperature profiles, it was possible to deduce the nature of the liquid flow-boiling during aerosol generation. The aerosol particle size went through a minimum, as energy was increased through the "optimal range." In the "energy excess" region, where additional energy increased PG vapor temperature and velocity, droplet sizes were increased primarily due to changes in the nucleation rates and supersaturation ratios affecting the nucleation and condensation processes occurring within the vapor jet. The in vitro MMAD of the PG aerosol changed as a function of the applied energy, suggesting that for any pharmaceutical application, the choice of applied energy is critical to deposition profile of the aerosol.

Keywords: Aerosol; Propylene glycol; Vaporization; Energy

1. Introduction

The capillary aerosol generator (CAG) is being developed as a novel aerosol generator for pharmaceutical inhalation drug delivery (Howell and Sweeney, 1998). In vitro studies with an early prototype version produced sub-micron condensation aerosols (Hindle et al., 1998). To enable site targeted pulmonary drug delivery, the particle size distributions of CAG generated aerosols could be controlled and modified using reservoir chambers (Hong et al., 2002). Typical formulations used with this device consist of a drug dissolved in a propylene glycol vehicle (PG). Propylene glycol is a GRAS excipient and has been used previously in nebulizer inhalation formulations. The mechanisms involved in generation of CAG aerosols include boiling, vaporization, nucleation, condensation and coagulation. To initiate aerosolization, the liquid formulation is electrically heated as it is simultaneously pumped through a micro-capillary tube. Multi-phase flow-boiling occurs as the liquid is carried through the capillary (Carey, 1992; Frankum et al., 1997; Lahey and Drew, 2001). The vapor jet exits the capillary and entrains and mixes with cooler surrounding air; supersaturation of the vapor then occurs and leads to nucleation, condensation and coagulation

* Corresponding author. Tel.: +1-804-828-6497; fax: +1-804-828-8359.
E-mail address: mhindle@vcu.edu (M. Hindle).

0378-5173/$ – see front matter © 2004 Elsevier B.V. All rights reserved.
doi:10.1016/j.ijpharm.2004.02.005

to form the aerosol (Lesniewski and Friedlander, 1995; Vatazhin et al., 1995; Ristovski et al., 1998).

Clearly, for the CAG, one of the most critical control parameters should be the amount of thermal energy supplied to boil and vaporize a known mass of liquid formulation. The energy supplied to the capillary, together with the formulation's mass flow rate, should determine the resultant capillary temperature profile, exiting vapor jet velocity and temperature. For efficient aerosolization, sufficient energy is believed to be required to produce a complete conversion of the liquid formulation into its gaseous state. In addition, it may also be desirable to achieve this phase change using the minimal amount of thermal energy to preclude unwanted thermal degradation. Therefore, it is necessary to find an energy window sufficient to vaporize the formulation but avoiding overheating.

In the simplest case, of a vehicle only formulation of propylene glycol, given its heat capacity and its vaporization enthalpy, the theoretical minimum energy required to heat a mass of liquid from room temperature to its boiling point, and completely convert it into vapor, can be calculated using the following equation (Perry et al., 1997):

$$\text{Energy} = \int_{\text{RT}}^{\text{BP}} mC_{p(T)}\,\mathrm{d}T + m\Delta H_{\text{V}} \quad (1)$$

where BP, RT, m, $C_{p(T)}$, T, and ΔH_{V} are boiling point, room temperature, mass, heat capacity at temperature, T, and the vaporization enthalpy at the boiling point, respectively. Eq. (1) served as a useful starting point for determining the amount of energy required by the capillary aerosol generator to aerosolize propylene glycol formulations. While solute or drug addition to vehicle is known to elevate the boiling point (Barrow, 1979) even heating PG alone by the CAG involves a number of additional "sensible" energy losses. The CAG operates in a dynamic flow-boiling mode as the liquid formulation is pumped through the capillary tube and the precise pressure regimes within the capillary are unknown. Furthermore, heat losses to the environment must be countered by performing experimental studies to determine total energy requirements. Extensive studies have investigated similar heat transfer and multi-phase flow-boiling phenomena in larger pipe systems for use in the nuclear power industry (Kwon and Chang, 1999; Bartel et al., 2001; Lahey and Drew, 2001; Yang et al., 2001). These have shown that flow within the channel is dependent upon a complex mix of the size and orientation of the channel, the mass flow rates of liquid and gas phases and the fluid properties of the system, together with the heat flux. The relevance of these macro studies to the micro-capillaries used in the CAG is unknown.

In this paper, we present an investigation of the effects of energy on the capillary aerosol generator's aerosolization efficiency for PG alone, using in vitro aerosol performance as the end-point, and temperature profiling to deduce and characterize some effects of varying the energy supply.

2. Materials and methods

2.1. Materials

Propylene glycol (USP) was obtained from Fisher Scientific Co., Fair Lawn, NJ (boiling point = 188 °C).

2.2. Aerosol generation

Fig. 1 shows a schematic diagram of the capillary aerosol generator. The system was equipped with a CAG capillary heater unit consisting of a 28 gauge stainless steel capillary (i.d. ≈ 180 μm) with a 44 mm heating zone and a plastic outer jacket designed to minimize thermal losses to the environment. The tip of the capillary was held flush with the end of the jacket. PG was pumped through the capillary at a mass flow rate of 3.5 mg/s for 10 s, thereby deliv-

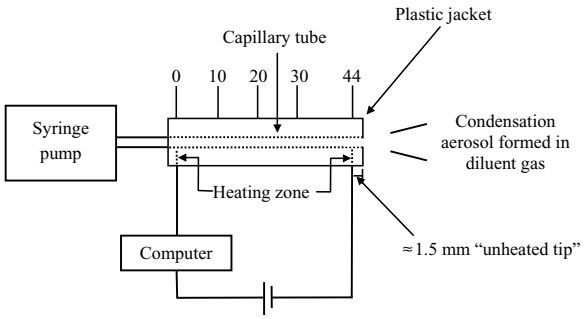

Fig. 1. Schematic diagram of the capillary aerosol generator. Values shown above the 44 mm capillary heating zone are distances (mm) from the positive power supply point.

ering 35 mg to the capillary in all experiments. The experimental run time of 10 s was selected to enable sufficient mass of PG to be delivered for analytical purposes. The wall of the stainless steel capillary was electrically heated by passing direct current through it from a power supply (0–8 V, 0–20 A). Conductive heating of the PG occurred as it flowed through the heated capillary. Upon exiting the capillary, the vapor jet entrained and mixed with ambient air producing an aerosol. All experiments were performed at ambient room temperature (21–24 °C) under relative humidity conditions ranging 14–60%.

2.2.1. Resistive heating

Control of the energy supply to CAG employed automated resistance-control and the relationship between the electrical resistance of a conductive heating element (the capillary itself) and temperature (Tuma, 1983):

$$R_T = R_0 + R_0\alpha_0 T \quad (2)$$

where the resistance, R, changes as a linear function of the temperature, T, and the material's temperature coefficient α_0, determined at 0 °C, respectively. In the present CAG format, the operator specifies a target resistance for maintenance during an aerosol generation experiment. DC current is chopped and supplied over computer-regulated durations to heat the capillary rapidly (typically $\leq$0.5 s) and subsequently to maintain the target resistance during the experiment. Selection of different target resistances produces the variation of power supply to the capillary. In order to investigate the effects of energy (power $\times$ time) on the aerosol characteristics of PG, the target resistance was varied between 0.90 and 1.01 Ω, corresponding to total power in the range of 3.3–8.4 W or 33–84 J of energy over each 10 s experiment. System resistance and supplied electrical energy were monitored as functions of time in each experiment. In separate experiments performed at a range of target resistances, propylene glycol aerosols were generated and the exterior wall temperature of the capillary was recorded using thermocouples (#5SC-TT-K-36–36, Omega Engineering Inc, Stamford, CT) placed 5, 10, 20, 30, 40, and 45 mm along the heating zone length of the capillary measured from the left; Fig. 1). In these experiments, thermocouples were also fixed in position 1, 15, and 30 mm from the capillary exit, on the vapor jet exit centerline, to measure the vapor jet temperature. Additionally, at selected energies, the temperature was recorded on the vapor jet centerline where the first visual appearance of aerosol was observed.

2.2.2. Energy corrections

Energy consumption in experiments in which thermocouples were applied to CAG is not reported here because small, but finite, sensible losses are contributed by application of the thermocouple(s). Furthermore, while the majority of the electrical energy supplied to the CAG was transferred to the PG, a fraction was expended heating the capillary wall and the air jacket surrounding the capillary. These energy losses were determined by performing a series of sham experiments (without PG presence or flow) at each target resistance and recording energy consumption. The energy consumed by the flowing PG was subsequently calculated by subtracting sham energy consumption from total energy supplied during aerosol generation at each target resistance.

2.3. Aerosol characterization

The MOUDI cascade impactor (MSP Corporation, Minneapolis, MN) was used to measure the aerodynamic particle size distribution of CAG aerosols (Marple et al., 1991). Aerosols were introduced into the MOUDI impactor operating at 30 $\pm$ 2 l/min via the USP stainless steel induction port positioned 3 cm from the capillary exit. After sampling, the impactor was disassembled and impaction substrates were analyzed gravimetrically to determine the total aerosol mass distribution using an analytical balance (Model AP250D, OHAUS Corporation, Florham Park, NJ). PG droplet size distributions were reported as the total aerosol mass distribution recovered from the MOUDI.

2.4. Data analysis

The fine particle fraction was defined as the aerosol mass with aerodynamic diameters less than 5.6 μm. Fine particle fraction was expressed as a percentage of nominal PG dose (35 mg) and used as a measure of aerosolization efficiency. The mass median aerodynamic diameter (MMAD) was defined as the particle size at the 50 percentile on a cumulative percent mass undersize distribution (D50) using linear inter-

polation. Geometric standard deviation (G.S.D.) was calculated as $(D84/D16)^{1/2}$ where D84 and D16 were determined similarly.

3. Results and discussion

3.1. Energy consumption and aerosol formation

During all experiments the target resistance was typically achieved ≤0.5 s after liquid supply was initiated. After this time, the mean measured resistance varied with coefficients of variation of ≤0.1% until, at 10 s, power to both the liquid pump and the CAG heater was switched off; heater resistance then returned rapidly to its resting (room temperature) state. Target resistances and measured average resistance agreed within <0.001 Ω in all experiments. During the 10-s pumping period, aerosols of PG were generated (see, for example, Fig. 6); in each case, cumulative energy supplied to the heater was recorded. Collected aerosols, sized by cascade impaction, were log-normally distributed in all cases with relatively narrow size distributions (δ_g values fell between 1.3 and 1.7). When sufficient or excess energy was supplied to completely vaporize the delivered PG bolus dose, the gravimetric recoveries of PG in the MOUDI were approximately >60% throughout and consistent with vapor losses during the 0.5 l/s aerosol sampling regime (∼12% was expected to remain in the vapor phase; Perry et al., 1997) and non-sampled surface losses known to occur in this cascade impactor and its induction port (Marple et al., 1991), together with losses on the capillary holder.

In order to estimate the thermal energy supplied to the PG during aerosolization, the energy consumed due to sensible loss during sham experiments was determined in the absence of PG over a range of target resistances. Typical results are shown for a thermocouple-instrumented CAG in Fig. 2, along with the resultant mean (external) capillary wall temperature at 30 mm along the heater in length (Fig. 1). Increasing the target resistance increased both the energy supplied to counteract sensible losses and the capillary temperature; the linear relationship between capillary temperature and target resistance (Eq. (2), Fig. 2) confirmed that the capillary heater unit responded well to "resistive control." When PG was pumped through the heated capillary (Fig. 1), it acted

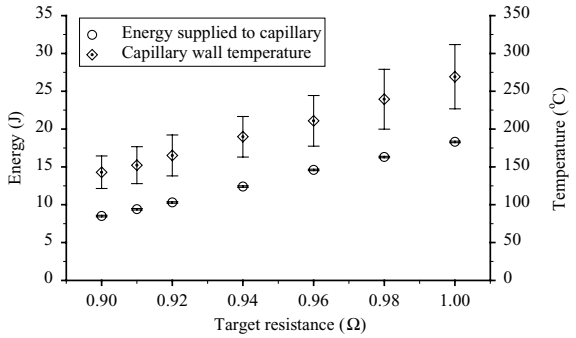

Fig. 2. The mean energy supplied to heat a thermocouple-instrumented capillary in a series of 10 s runs performed at different target resistances. Mean capillary exterior wall temperatures were measured 30 mm along the heater length (Fig. 1; error bars represent S.D.s, $n = 3$).

as a coolant so that extra energy, in addition to that supplied during sham experiments was demanded, in order to maintain the selected target resistance. This extra energy was supplied to heat the liquid, convert it to vapor and, if the selected resistance target was high enough, to heat the vapor itself. Over the range of resistances studied, the sham energy, representing heat lost to the apparatus and the environment, was an effectively constant proportion (17.6 ± 1.3%) of the total supplied during the aerosolization of PG. Thus, energy supplied to PG during aerosolization studies (plotted in Figs. 4 and 5 along with the corresponding resistance targets) was calculated by subtracting the sham energy determined at the same target resistance from the total supplied during the experiment. These calculated energies were used to more closely reflect the amount of energy consumed by the flowing PG in the remainder of this discussion.

Assuming that boiling occurs homogeneously at 1 atm pressure, that heat flux is uniform over time and space, and that both phases are incompressible fluids (Delmastro et al., 2001), a theoretical calculation of the energy required to vaporize the constant mass of propylene glycol (35 mg) used in this study was performed using Eq. (1), where values for the heat capacity and vaporization enthalpy of propylene glycol were as reported by Perry et al. (1997); assuming a boiling point of 188 °C and a room temperature of 22 °C vaporization should consume 43 J (18 J to heat the liquid to 188 °C and 25 J to effect the phase transformation).

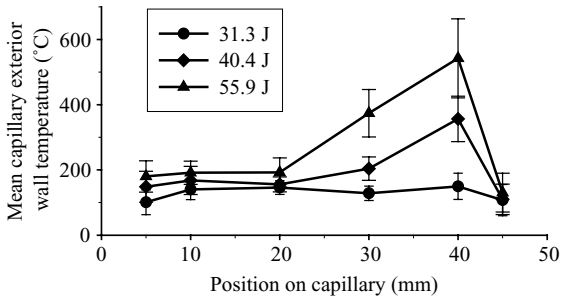

Fig. 3. The capillary exterior wall temperature measured during the application of 31.3, 40.4, and 55.9 J to PG during each 10 s experiment at 5, 10, 20, 30, 40, and 45 mm along the heated capillary (Fig. 1; error bars represent S.D.s).

3.2. Capillary characteristics as a function of energy supplied to PG

Simultaneous inspection of Figs. 3–5 show that the theoretical, 43 J, energy requirement to raise the temperature of each 35 mg bolus of PG, and vaporize it, was in agreement with the measured parameters in this study. Discontinuities in PG aerosol size, vapor jet temperature, and capillary heater temperature profiles were all apparent at or near this energy supply value. Values for fine particle fraction (an indicator of complete vaporization) reached a plateau, MMAD values passed through a broad minimum and the gradient, with which the temperature of the PG vapor jet changed with energy, increased sharply. This latter

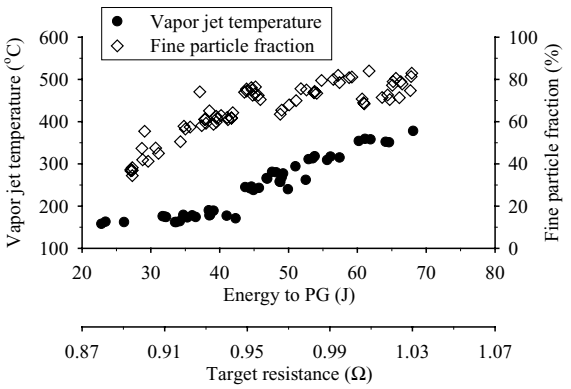

Fig. 4. Mass fraction of PG aerosol with aerodynamic diameters <5.6 μm expressed as a percentage of nominal PG dose, plotted vs. energy supplied to PG. Also plotted was propylene glycol vapor jet temperature measured 1 mm from the capillary exit vs. energy supplied to PG.

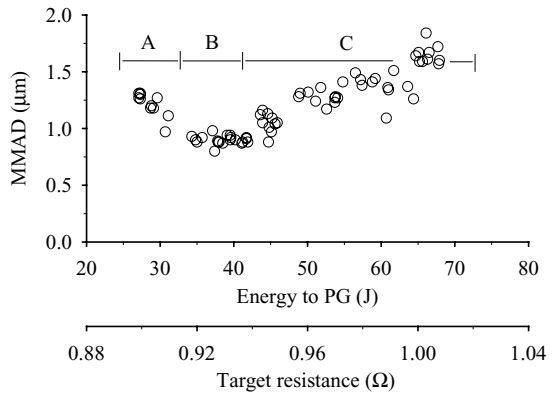

Fig. 5. The MMAD of PG aerosols vs. energy supplied to PG. The zones A, B, and C correspond to regions in the energy profile discussed in the text.

phenomenon, taken with the appearance of the aerosol formation process (Fig. 6; note that the aerosol cloud formation occurred further from the jet as energy was increased) was consistent with excess energy being used to heat the vapor. Within the capillary, concurrent changes in its temperature profile (Fig. 3) were broadly indicative of a liquid-to-vapor transition which occurred earlier in the capillary (Fig. 1) as the energy supply was increased. This vapor is heated to a greater extent, the earlier in the capillary it is produced. The net effect is, that a superheated vapor nucleates and condenses at distances further from the capillary tip as it takes longer for the vapor to cool from these elevated temperatures (Fig. 6). Notably, control of the overall resistance of the heater corresponded to control of its temperature "average" (Fig. 2) although temperature variations along its length could be influenced by PG flow and CAG design. In Fig. 3, at 45 mm, the thermocouple was placed beyond the 44 mm heating zone in this CAG design manifestation (Fig. 1), and wall temperatures were generally low and independent of the energy supply at the exit of the capillary. At low energies, in which incomplete vaporization was indicated (Figs. 4 and 5), temperature profiles were flat and roughly consistent with the continuous contact of boiling PG passing through the capillary heater. As the power supply was increased, wall temperatures deviated from this "boiling plateau," indicating the internal presence of an increasing vapor content, at points earlier in the heating zone (Fig. 3). These deviations, and the significant temperature elevations close to the

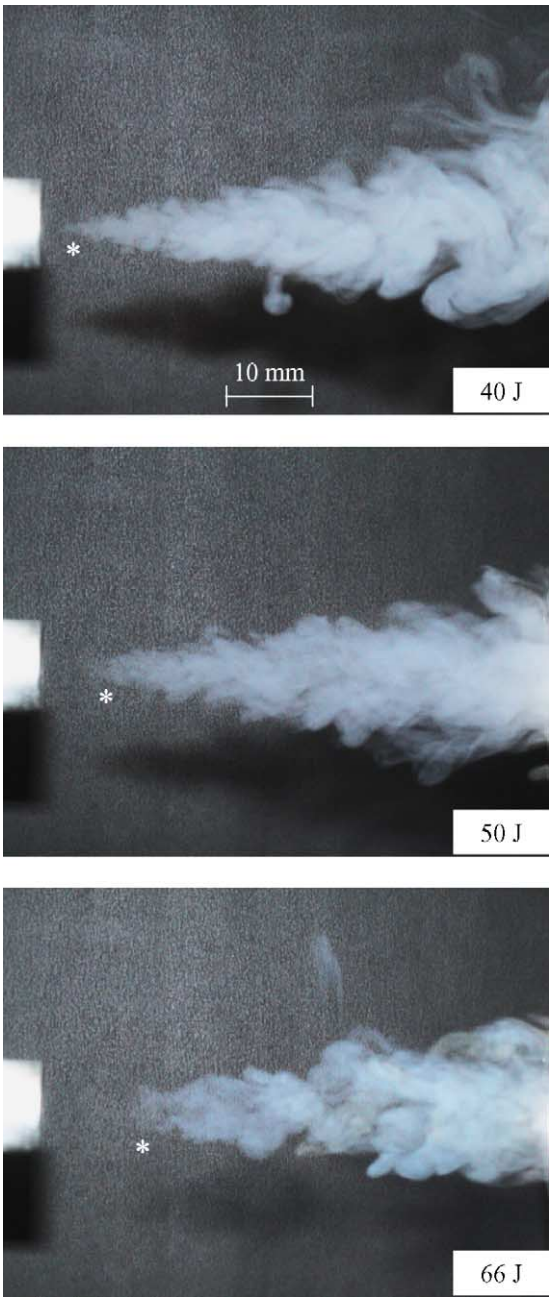

Fig. 6. Typical vapor jet images of CAG aerosol generated at increasing energies. The angle formed by the jet boundaries varied in the range of 20–30°, comparable to the 26° reported by Lesniewski and Koch (1998) for a turbulent jet. At higher energies higher vapor exit temperatures and velocities pushed the condensation process further downstream as shown by asterisk (∗).

exit of this capillary design were consistent with the combined effects of boiling point elevations associated with increased internal pressures and superheating of the vapor during its passage to the open end of the capillary.

Efficient aerosol generation was thus dependent upon the complete vaporization of the liquid formulation; once the minimum amount of energy required was exceeded, aerosol characteristics could be changed (Fig. 5). Due to the ultrafine characteristics of CAG aerosols (usually $<3\,\mu m$), the fine particle fraction will not change once sufficient energy is supplied to enable complete liquid–vapor transition. A maximal FPF will be achieved once all the liquid has been vaporized. However, the aerosol particle size is still subject to changes due to the superheating of the vapor within the capillary, which will alter its nucleation and condensation mechanism on exiting the capillary. Superheating of the vapor can only take place when all the liquid has been vaporized within the capillary. Heating of the formulation as it is pumped through the capillary can probably be visualized by considering the formulation flow inside the capillary as flow segments in a continuum; as a flow segment travels along the capillary, it increases in temperature through convective heating. As long as liquid remains in contact with the capillary wall, the wall temperature should be related to the temperature of the liquid. For any segment, the liquid closest to the capillary wall should be heated more efficiently than the flow stream in the center of the capillary, and thus it is this portion of a segment that should vaporize first (Carey, 1992).

3.3. Aerosol characteristics as a function of energy supplied to PG

Three broad regions of the MMAD versus energy profile for this capillary design are shown graphically in Fig. 5 as A, B, and C. These corresponded, in terms of the energy demand of PG to “energy starved,” “energy sufficient,” and “energy excess” situations, respectively. In region A, the “energy starved” situation, simultaneous pumping (while heating sub-optimally), ensured partial vaporization along with some “heated spray formation.” This effect was observed most readily in Figs. 4 and 5 as a gradual increase in fine droplet formation and a decrease in MMAD as increasing energy supply reduced the aerosol fraction formed as a

"heated spray." Collectively, the mean (S.D.) MMAD of region A was 1.21 (0.10) μm. The mean MMAD is presented for comparative purposes of region A with other regions, however, it should be noted that the aim of these studies was not to investigate aerosol performance reproducibility at specific applied energies, rather to investigate the continuum effects of increasing the applied energy. The aerosols generated at these lower applied energies, could be favorably compared to conventional technologies such as MDI's and DPI's, CAG aerosol FPF's ranged from 40–60%, with a mean MMAD of 1.21 μm. Finally, in this "energy starved" region, the apparent jet exit temperature was effectively constant and consistent with the known boiling point of PG (Fig. 4).

The "energy sufficient" region B (Fig. 5) showed a nadir in MMAD but it was only at the upper end of the region, and the commencement of region C, that the fine droplet formation truly began to plateau (Fig. 4). The mean (S.D.) MMAD of region B was 0.90 (0.04) μm, there was a statistically significant decrease from that of region A ($P < 0.05$; Mann–Whitney Rank Sum Test). Such an energy regime may be considered optimal, given that this produced the maximum fine particle fraction at the lowest applied energy (thus minimizing adverse thermal effects on both the vehicle and any active ingredient). Pulmonary deposition efficiencies for a 0.9 μm aerosol would be expected to be high. In the capillary design employed for these experiments, there appeared to be a need to employ a temperature profile (e.g. Fig. 3; 40.4 J) in which the PG vapor was sufficiently heated, at the capillary exit, to avoid losses at its cooler tip, and on the stainless steel induction port leading to the MOUDI cascade impactor (Marple et al., 1991; Stein and Gabrio, 2000). Lower temperatures were observed at each end of the capillary employed in these experiments, due to the presence of heat sinks at the electrical joints on the capillary.

In the "energy excess" region C, PG became completely vaporized and, due to the poor heat transfer coefficient and low heat capacity of the vapor, significant increases in wall temperature were seen which were indicative of the extent of "dryout" in the capillary, and the degree of superheating to which the vapor was exposed (Fig. 3) (Caira et al., 1995; Castrogiovanni and Sforza, 1997). Because the volume of each flow segment was confined by the capillary wall and flow segments immediately ahead and behind, the internal pressures must also increase with increasing energy supply. As a result the adiabatic vapor expansion which occurs at or within the capillary exit, accelerates the vapor to form a jet. Continuing to apply further energy, in excess of that required for vaporization, thus increased capillary wall temperature, the vapor exit temperature, velocity (Fig. 6) and aerosol MMAD (Fig. 5). For comparative purposes, the mean (S.D.) MMAD in this region was 1.34 (0.23) μm, this was a statistically significant increase in aerosol MMAD compared to region B ($P < 0.05$; Mann–Whitney Rank Sum Test).

Energy induced aerosol particle size changes have been described, in which the CAG generated aerosol particle size was observed to first decrease and then increase when the applied energy was increased through the optimal applied energy range. Although not the specific aim of this study, also of interest, is the reproducibility of the CAG to generate aerosols under a constant energy condition. The mean (%R.S.D.) MMAD and %FPF are reported at discrete energy values in region A, B, and C, respectively. In region A, at 27.2 (S.D. = 0.1) J ($n = 6$), the mean (%R.S.D.) MMAD and %FPF were 1.3 μm (1.8%) and 36.7 % (3.8%). Similar values for region B, at 36.6 (S.D. = 0.4) J ($n = 5$) were 0.9 μm (2.2%) and 61.1 % (2.9%), respectively. Finally, for region C, at 66.6 (S.D. = 1.2) J ($n = 5$) were 1.6 μm (1.9 %) and 80.5 % (2.1%), respectively. It should be noted that the reproducibility of CAG aerosolization is a function of the position on the energy profile and hence the efficiency of the liquid–vapor transition.

3.4. Propylene glycol aerosol formation and size evolution in regions B and C (Fig. 5)

To comprehend the changes in aerosol particle size as a function of energy, it is essential to consider the complex processes that take place during the vapor to droplet phase transition in the vapor and aerosol jet expelled from the heated capillary. PG aerosol formation in this region produced clouds of increasing median size as the energy supply to the CAG was increased (Fig. 5). Although coagulation effects could not be excluded, it was highly unlikely to be responsible for the size changes given the PG mass flow rate, sampling air flow rate and the aerosol transition time

from capillary tip to the MOUDI stages. These conditions favored a nucleation dominated aerosol formation mechanism rather than a coagulation dominated process (Lesniewski and Koch, 1998). Another possible confounding factor, given the hygroscopic properties of propylene glycol was the possibility that the measured particle size distribution was affected by the ambient relative humidity. However, Hong et al. (2002) showed previously that at relative humidities in the range of 24–70% RH, there was no significant effect on the measured aerosol particle size (Hong et al., 2002). The observed changes in particle size could best be explained based on the effectively linear dependence of nucleation rate on supersaturation ratio (Hinds, 1982; Kane and El-Shall, 1996) for homogeneously nucleating and condensing PG in vapor jets with different temperature profiles (generated at different CAG energy supply settings). Based on the position in the jet, at which the aerosol cloud formation commenced (the distance from the exit increased with increasing energy supply), effective nucleation rates appeared to decrease by a factor of about 5.6, as the energy supply to each PG bolus was increased from 40 to 66 J. The reasoning that follows, while necessarily speculative, was based on the relevant literature and the critical experimental observations made in this study as shown in Table 1 and Figs. 5 and 6.

To begin, observe that the vapor-to-droplet conversion in the jet escaping from the capillary exit involves adiabatic expansion, turbulent mixing and resultant cooling, due both to expansion and dilution with entrained room air. Reynold's numbers in the vapor at the capillary exit are of the order of 2000 or more (Gupta et al., 2003) and these increased with the exit temperature of the vapor (Fig. 4), because of its increasing linear vapor velocity at the exit (ranging approximately 70–100 m/s between 40 and 66 J). Vapor cooling from CAG is primarily due to turbulent mixing with cool air (adiabatic expansion has only a small effect) and it is known that condensation aerosol formation in circumstances such as these is complete within 20–50 nozzle diameters (Nicolaon et al., 1971), 4–10 cm in this case, using an effective nozzle diameter of 0.2 cm. The classic work of Hinze and Van Der Hegge Zijnen (1949) on turbulent gas jet mixing with quiet air, following discharge from a rectangular orifice, can also be applied directly. Those workers showed that temperatures measured at the centerline of a similar gas jet remained close to the vapor's exit temperature, T_0, for 3–4 nozzle diameters, after which turbulent mixing with entrained cooler air caused an exponential decay of temperature, T, falling to around ambient, at 40 nozzle diameters. Temperatures measured radially from the jet centerline, at any fixed distance from the nozzle, were also shown to decrease exponentially toward that of the environment. These steady-state temperature profiles are formed within the zone of turbulent mixing between the hot vapor and the entrained air in an expanding cone with an angle between 20 and 30° (this study, Fig. 6); a result consistent with the 26° angle reported for a turbulent jet (Lesniewski and Koch, 1998). Clearly, PG vapor concentration also de-

Table 1
Relationships between aerosol nucleation, temperature, and distance in PG vapor jets formed by the CAG in the "energy sufficient and excess regions" B and C of Fig. 5

Energy[a] (J)	$T_{0.1}$[b] (°C)	T_{nucl}[c] (°C)	X_{nucl}[d] (cm)	$[PG]_{nucl}$[e]	MMAD/$MMAD_{min}$[f]	RSR[g]	RNR[h]
40	180	114	0.3	0.98	1.0	1.0	1.0
50	260	115	0.7	0.19	1.3	0.18	0.42
66	370	103	1.2	0.06	1.8	0.10	0.18

[a] Supplied to PG, experimentally determined.
[b] Temperature at jet centerline 0.1 cm from exit (Fig. 4), experimentally determined.
[c] Temperature at nucleation position on jet centerline, experimentally determined.
[d] Horizontal distance along jet centerline, X, for nucleation.
[e] Relative PG vapor concentration at position of nucleation (assuming volume elements increase as a linear function of X^2 and a diverging jet angle = 26°).
[f] Relative mass median diameter (Fig. 5).
[g] Relative saturation ratio (RSR), calculated based on PG vapor pressure at T_{nucl} and $[PG]_{nucl}$.
[h] Relative nucleation rate (RNR), calculated based on experimental MMAD (Fig. 5) and the observation of constant PG recovery (Fig. 4), monodispersity of the aerosol was assumed to allow simplified calculation.

creases with distance from the exit, in this case in inverse proportion to the square of the increasing distance, X^2 (because the volume of each "jet cone element" must increase with the square of the jet's diameter).

Following this preamble, the likely nucleation rate versus energy supply relationship shown in Table 1 can be interpreted mechanistically. The distance from the exit, X_{nucl}, at which aerosol formation began, appeared to be a linear function of the energy supplied to the formulation, and an indicator of the position at which the critical supersaturation ratio was exceeded, thereby enabling PG aerosol nucleation and condensation (Hinds, 1982). The validity of this statement presumes that heterogeneous nucleation due to room air particulates (10^3–$10^5\,cm^{-3}$) was negligible while homogeneous nucleation due to supersaturation and growth of PG was dominant (Bricard and Pradel, 1966; Gupta et al., 2003; Hindle et al., 1998). It followed that for the observed increase in aerosol median diameter with increasing energy supply (Table 1), that the relative nucleation rate (RNR; proportional to total number concentration) must fall, given the effectively constant recovery of PG seen in regions B and C (Fig. 5) of this study. In the energy range shown in Table 1, both the temperature and the concentration of PG at the observed point of aerosol formation, T_{nucl} and $[PG]_{nucl}$, respectively, brought about changes in the critical supersaturation ratio at which homogeneous nucleation occurred. It is interesting to note that the values of T_{nucl} were similar, calculated values for the relative supersaturation ratio, RSR (Table 1) fell in line with the decrease of RNR and corresponding increase in MMADs (Hinds, 1982). The decrease of RNR is apparently correlated with the decreasing visual aerosol jet density caused by the increase of applied energy, the aerosol jet density can be better differentiated by paying attention to the darkness of its shadow (Fig. 6). The numerical values relating relative supersaturation ratios to nucleation rates appeared to agree relatively well in Table 1, the supersaturation dependency of nucleation was consistent with the results, showing that there was little reason to doubt the domination of homogeneous nucleation as the main mechanism for PG aerosol formation from CAG, and that this was the mechanism of control for aerosol size at different applied energies.

4. Conclusion

The CAG generated aerosol particle size was observed to first decrease and then increase when the applied energy was increased through the optimal applied energy range. Increasing the applied energy also improved the fine particle fraction of the formed aerosols at lower applied energies. This study also illustrated that through adjusting the applied energy input, it may be possible to modulate the CAG aerosols to target a particular particle size distribution. Additionally, through the auxiliary capillary wall and vapor temperature profiles investigations, this study explored and elucidated the CAG aerosol formation mechanism, this enhances the understanding of CAG aerosol generation.

Acknowledgements

This research was supported by Chrysalis Technologies, Inc. We are grateful to Dr. Samy El-Shall for his review and comments on portions of this manuscript.

References

Barrow, G.M., 1979. Physical Chemistry, 4th ed. McGraw-Hill Book Company, New York.

Bartel, M.D., Ishii, M., Masukawa, T., Mi, Y., Situ, R., 2001. Interfacial area measurements in subcooled flow boiling. Nucl. Eng. Des. 210, 135–155.

Bricard, J., Pradel, J., 1966. Electric charge and radioactivity of naturally occurring aerosols. In: Davies, C.N. (Ed.), Aerosol Science. Academic Press, New York, p. 87.

Caira, M., Caruso, G., Naviglio, A., 1995. A correlation to predict CHF in subcooled flow boiling. Int. J. Heat Mass Transfer 22, 35–45.

Carey, V.P., 1992. Liquid–Vapor Phase-Change Phenomena. Hemisphere Pub. Corp., Washington, DC.

Castrogiovanni, A., Sforza, P.M., 1997. A genetic algorithm model for high heat flux flow boiling. Exp. Thermal Fluid Sci. 15, 193–201.

Delmastro, D., Juanicó, L., Clausse, A., 2001. A delay theory for boiling flow stability analysis. Int. J. Multiphase Flow 27, 657–671.

Frankum, D.P., Wadekar, V.V., Azzopardi, B.J., 1997. Two phase flow patterns for evaporating flow. Exp. Thermal Fluid Sci. 15, 183–192.

Gupta, R., Hindle, M., Byron, P.R., Cox, K.A., McRae, D.D., 2003. Investigation of a novel condensation aerosol gnerator: solute and solvent effects. Aerosol Sci. Tech. 37, 672–681.

Hindle, M., Byron, P.R., Jashnani, R.N., Howell, T.M., Cox, K.A., 1998. High efficiency fine particle generation using novel condensation technology. In: Dalby, R.N., Byron, P.R., Farr, S.J. (Eds.), Proceedings of Respiratory Drug Delivery, vol. VI. Interpharm Press, Inc., Buffalo Grove, IL, pp. 97–102.

Hinds, W.C., 1982. Aerosol Technology: Properties, Behavior, and Measurement of Airborne Particles. John Wiley & Sons, Inc., New York.

Hinze, J.O., Van Der Hegge Zijnen, B.G., 1949. Transfer of heat and matter in the turbulent mixing zone of an axially symmetrical jet. Appl. Sci. Res. A1, 435–461.

Hong, J.N., Hindle, M., Byron, P.R., 2002. Coagulation of model inhalation aerosols in reservoir chambers: behaviour of condensed systems of solute and propylene glycol. J. Aerosol Med. 15, 359–368.

Howell, T.M., Sweeney, W.R., 1998. Aerosol and a method and apparatus for generating an aerosol. United States Patent 5/743,251.

Kane, D., El-Shall, M.S., 1996. Condensation of supersaturated vapors of hydrogen bonding molecules: ethylene glycol, propylene glycol, trimethylene glycol, and glycerol. J. Chem. Phys. 105, 7617–7631.

Kwon, Y.M., Chang, S.H., 1999. A mechanistic critical heat flux model for wide range of subcooled and low quality flow boiling. Nucl. Eng. Des. 188, 27–47.

Lahey, R.T., Drew, D.A., 2001. The analysis of two-phase flow and heat transfer using a multidimensional, four field, two-fluid model. Nucl. Eng. Des. 204, 29–44.

Lesniewski, T., Friedlander, S.K., 1995. The effect of turbulence on rates of particle formation by homogeneous nucleation. Aerosol Sci. Tech. 23, 174–182.

Lesniewski, T.K., Koch, W., 1998. Production of rounded Ti- and AI-hydroxide particles in a turbulent jet by coagulation-controlled growth followed by rapid coalescence. J. Aerosol Sci. 29, 81–98.

Marple, V.A., Rubow, K.L., Behm, S.M., 1991. A Micro Orifice Uniform Deposit Impactor (MOUDI): description, calibration, and use. Aerosol Sci. Tech. 14, 434–446.

Nicolaon, G., Cooke, D.D., Davis, E.J., Kerker, M., Matijević, E., 1971. A new liquid aerosol generator II. The effect of reheating and studies on the condensation zone. J. Colloid Interface Sci. 35, 490–501.

Perry, R.H., Green, D.W., Maloney, J.O., 1997. Perry's Chemical Engineers' Handbook. McGraw-Hill, New York.

Ristovski, Z.D., Morawska, L., Bofinger, N.D., 1998. Investigation of a modified Sinclair-La Mer aerosol generator in the submicrometer range. J. Aerosol Sci. 29, 799–809.

Stein, S.W., Gabrio, B.J., 2000. Understanding throat deposition during cascade impactor testing. In: Dalby, R.N., Byron, P.R., Farr, S.J., Peart, J. (Eds.), Proceedings of Respiratory Drug Delivery VII, vol. II. Davis Horwood International Publishing, Ltd., Raleigh, NC, pp. 287–290.

Tuma, J.J., 1983. Handbook of Physical Calculations, 2nd ed. McGraw-Hill, New York.

Vatazhin, A., Lebedev, A., Likhter, V., Shulgin, V., Sorokin, A., 1995. Turbulent air-steam jets with a condensed dispersed phase: theory, experiment, numerical modeling. J. Aerosol Sci. 26, 71–93.

Yang, Z.L., Dinh, T.N., Nourgaliev, R.R., Sehgal, B.R., 2001. Numerical investigation of boiling regime transition mechanism by a Lattice-Boltzmann model. Nucl. Eng. Des. 204, 143–153.